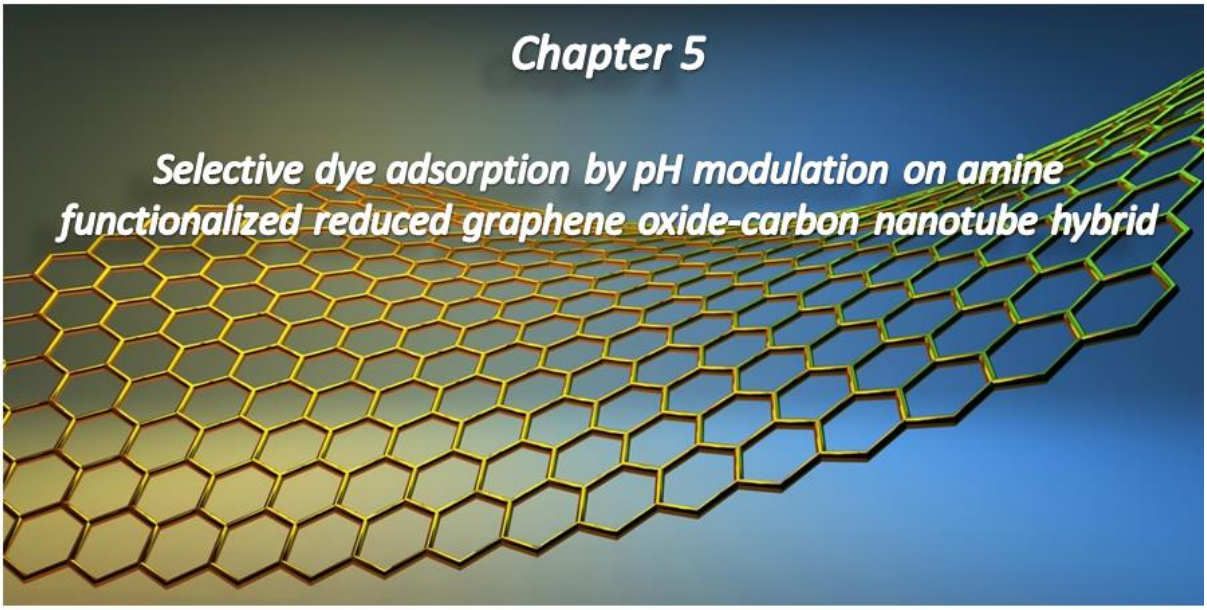

GRAPHICAL ABSTRACT

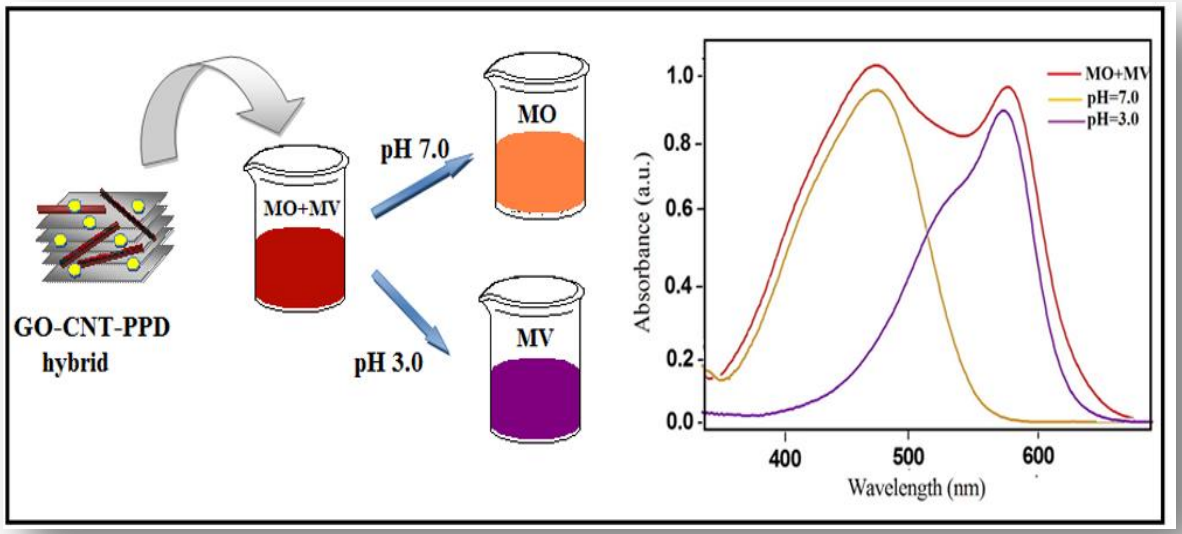

***p*-phenylenediamine and MWCNT functionalized graphene can selectively adsorb dye by modulating the pH from their mixture; at pH 7.0, it removes 99.5% methyl violet selectively, while at pH 3.0, it removes methyl orange selectively having 98% removal efficiency.**

5.1 Introduction

Dyes have become indispensable chemicals for a variety of industries such as dye synthesis, textile, printing, paper, electroplating, pulp mill, food, paints, polymers, cosmetics and the highly sophisticated biotechnology industry. Unfortunately, most of them are toxic, carcinogenic and teratogenic to human beings [1]. Waste dyes are the major source of water pollution. Methyl violet (MV) and methyl orange (MO) are widely used cationic and anionic dyes in several industries and research laboratories. Hence, MV and MO were selected as representative target pollutants for this study. Now a day, several physical, chemical and biological methods have been used in water treatment, such as adsorption [2, 3], membrane separation [4], photocatalytic degradation [5], ozone treatment [6], oxidation [7, 8], ion exchange [9, 10] and biological treatment [11]. Among these methods, adsorption is the most widely used method because of its low cost, ease of operation, high efficiency and simplicity in design and operation.

Various carbon based materials such as activated carbon [12], CNT [13], porous carbon [14], GO, graphene [15-17] and GS [18] have been studied for adsorption of various dyes from water because of their excellent physiochemical and mechanical properties. Although, activated carbon has high specific surface area, it is flammable, difficult to regenerate and their weak hydrophilic properties make weak interaction between the adsorbent and dyes [19]. Due to hollow and layered structures, CNTs have been utilized for the adsorption of a large number of different organic compounds from water. The multiwall carbon nanotube has been used as an efficient adsorbent for the removal of several dyes such as alizarin red s, morin, reactive blue 4 and acid red 183 from wastewater [20-23]. However, CNTs have relatively lower specific surface area than activated carbon. GO nanosheets are decorated with numbers of oxygen containing functional group such as hydroxyl, carboxylic, carbonyl, and epoxide groups which imparts negative charge density to it in aqueous solution. Their high water solubility and electrostatic interaction of GO with adsorbate makes them a material of great interest in adsorption of charged species [15, 23, 24]. Many research groups have reported the use

---

This part of the thesis is published in

Sarkar, C., Bora, C., and Dolui, S. K. Industrial & Engineering Chemistry Research, 53(42):16148-16155, 2014.

of GO as adsorbent material for removal of various dyes such as MV, rhodamine B, orange G, methylene blue and methyl green from aqueous solutions [15, 25]. Although a large number studies have been reported for effective dye adsorption, very few studies emphasized on selective dye adsorption from their mixture [22, 26]. Ho, K. Y. et al. demonstrated ordered mesoporous silica (OMS) could be used as adsorbents for removal of acid blue 25 and methylene blue dyes selectively from their mixture [26]. The amino-containing OMS-NH_2 adsorbent can selectively remove acid blue 25, while, the OMS-COOH can absorb methylene blue from their mixture.

Recently, a new group of materials have been synthesized from hybridization of CNTs and GO (GO-CNT) which showed better properties than their individual counterparts [27-31]. However, dye adsorption efficiency of GO-CNT hybrid was inferior to that of reduced graphene oxide-carbon nanotube hybrid (rGO-CNT) [32]. The reduction of GO required some highly toxic and harmful reducing agents such hydrazine hydrate [33] and sodium borohydride [34]. Therefore, to improve the dye adsorption properties of GO-CNT hybrid, development of suitable reduction process is essential by exploring simultaneous functionalization and followed by reduction of GO. Recently, simultaneous reduction, functionalisation and stitching of GO have been carried out with ethylemediamine [35] and *p*-phenylenediamine (PPD) [36] for various applications.

In the present work, a novel chemical approach is established to functionalize GO-CNT hybrid by PPD followed by reduction of GO. This approach eliminates use of toxic and harmful chemicals used for the synthesis of rGO. The aim of this study is to explore the selective dye adsorption efficiency of rGO-CNT-PPD from the mixture of MV and MO solution by pH modulation. The adsorption properties of the hybrid for selective removal of MV and MO from their mixture were investigated under different experimental conditions. The effects of pH, contact time and temperature on the adsorption capacity have been investigated. Also the adsorption kinetics and isotherms has been estimated to evaluate the adsorption capacity and understand the mechanism of adsorption of rGO-CNT-PPD hybrid towards MV and MO.

5.2 Experimental Section

5.2.1 Chemicals

Multiwall carbon nanotube (Redex Technologies Pvt. Ltd. Ghaziabad UP India), graphite power (<20 micron, Aldrich) were used as received. Sodium nitrate ($NaNO_3$),

potassium permanganate ($KMNO_4$), hydrogen peroxide (50% v/v), sodium dodecyl sulphate, concentrated sulfuric acid (98%), hydrochloric acid and ethanol (99%) were procured from Merck. Methyl violet (Merck) and methyl orange (Merck) were recrystallized.

5.2.2. Preparation of graphene oxide (GO), GO-CNT hybrid

GO was synthesized from natural graphite powder using Hummers method [37]. GO-CNT hybrid was synthesized by ultrasonication of GO and CNT. In this process, MWCNT (10 mg) was dispersed in 0.5 wt % sodium dodecyl sulphate (20mL) by ultrasonication to form a homogeneous dispersion. GO (30mg) was dispersed in 20mLwater by ultrasonication. These two homogeneous dispersions were mixed and ultrasonicated for 30min. Then GO-MWCNT dispersion was centrifuged and washed several times with distilled water and finally after drying GO-CNT hybrid was obtained as a black solid.

5.2.3 Preparation of rGO-CNT-PPD hybrid

A simultaneous reduction and functionalisation of GO-CNT hybrid was carried out by PPD. In a typical process, PPD-ethanol (0.3g in 100mL) solution was mixed with equal volumes of the GO-CNT (0.1g in 100mL) dispersion prepared in water. The mixture was then refluxed at 80 °C for 24 h with stirring. The obtained solution was centrifuged and washed repeatedly with a 1:1 ethanol/water solution until the centrifugal liquid became colourless and finally dried to obtained rGO-CNT-PPD hybrid. Steps involved in the synthesis of rGO-CNT-PPD hybrid are shown in Scheme S1. For comparison, rGO-PPD hybrid and CNT-PPD hybrid were also synthesized. They were synthesized following the same procedure used in the synthesis of rGO-CNT-PPD hybrid. In the synthesis of CNT-PPD hybrid, CNT was dispersed in 0.5 wt % sodium dodecyl sulphate.

5.2.5 Characterization

FTIR, XRD, SEM and TEM analyses were carried out for characterization of the samples. The TEM measurements were carried out by using FEI 200KV TEM model Technai G2 F2OS-TWIN instrument.

5.2.6 Batch Adsorption Experiments

Selective adsorption properties of rGO-CNT-PPD hybrid were investigated for mixture of two different organic dyes, MO and MV using batch adsorption experiment. 0.005 g of the hybrid adsorbent was added to 50 mL of mixture solution having 1:1 MO/MV ratio with 30 mg/L concentration of each dye and the mixture was stirred for 120 min. The adsorbent was separated by centrifugation and the concentrations of each dye after adsorption were determined by using uv-vis spectrophotometer at 464 nm and 582 nm wavelengths for MO and MV respectively. The effect of pH on the adsorption was studied with an initial dye concentration of 30 mg/L for both dyes in a pH range of 1.0−11.0 at 298 K. The pH value of the mixed solution was adjusted with a 0.1 M HCl or 0.1 M NaOH solution. All other experiments for selective adsorption of MV and MO were performed under pH value 7.0 and 3.0 respectively. Kinetic experiments were carried out with an initial dye concentration of 30 mg/L for both dyes at room temperature, to determine the minimum time required for adsorption to reach steady state. The concentrations of dyes after adsorption were measured at regular time intervals from 15 to 180 min. The adsorption isotherm experiments were obtained by adding 0.005 g of adsorbent in 50 mL of the aqueous solution with initial dye concentration of 2-50 mg/L. The adsorption capacity (q_e, mg/g) of the hybrid and the percentage of removal of dyes by the adsorbent can be calculated by applying equations (1) and (2), respectively:

$$q_e = (C_0\text{-}C_e)v/m \quad (1)$$

$$\% \text{ Removal} = 100 \times (C_0\text{-}C_e) / C_0 \quad (2)$$

Where, C_0 and C_e represent the initial and equilibrium dye concentrations of aqueous solution (mg/L), v is the volume of the solution (L), and m is the mass of the adsorbent (g).

5.2.7. Desorption experiments

After adsorption experiments, the adsorbent was separated by centrifugation and added into 50 mL of ethanol and stirred for 120 minutes at pH 7.0 for MV. The adsorbent was collected by centrifugation and reused for another adsorption-desorption cycle. The concentration of the supernatant dye solution was examined by uv–vis spectroscopy. The cycle was repeated for five times following same procedure.

5.3 Results and discussion

5.3.1 Characterization of rGO-CNT-PPD hybrid

5.3.1.1 FTIR study

Fig.5.1 shows the FTIR spectra of GO, MWCNT, GO-CNT, rGO-CNT-PPD, rGO-PPD and CNT-PPD. In the FTIR spectrum of GO (Fig.5.1a), we observe the absorption peaks at 3457 cm^{-1} for O–H stretching vibration, 1708 cm^{-1} for C=O stretching vibration, 1572 cm^{-1} for aromatic C=C stretching vibration, 1367 cm^{-1} for C–OH stretching vibration and 1062 cm^{-1} for C–O stretching vibration. Pristine MWCNT shows a strong absorption band at 3456 cm^{-1} due to O−H stretching vibration, a weak band at 1637 cm^{-1} for C=O stretching vibration and a weak band at 1156 cm^{-1} for C-O stretching vibration (Fig.5.1b). The FTIR spectrum of GO-CNT hybrid (Fig.5.1c) shows peaks for both GO and CNT which indicates the successful formation of GO-CNT hybrid. Moreover, we have observed little shifting of the peaks in the FTIR spectrum of GO-CNT hybrid which indicates the interaction between GO and CNT. Functionalization on GO-CNT hybrid by PPD as well as reduction of GO were confirmed by FTIR spectrum of rGO-CNT-PPD hybrid as shown in fig.1d. This spectrum shows that the peak intensity of C=O, C-OH and C-O groups decrease significantly, indicating reduction of GO by PPD. Again, shifting of the peaks of GO-CNT hybrid in the FTIR spectrum of rGO-CNT-PPD hybrid confirms interaction between them. Some new peaks appeared at 3410, 3360, 1610, and 770 cm^{-1} corresponding to $-NH_2$ double stretching, N−H bending, and N−H wagging vibrations, respectively, confirming functionalization of GO-CNT hybrid with PPD. A strong peak arises at 1168 cm^{-1} due to C−N stretching vibration mode which confirms the formation of C−NH−C bands. Thus FTIR analysis indicated simultaneous reduction of GO and amine functionalization on GO-CNT hybrid. For comparison, FTIR spectra of rGO-PPD, CNT-PPD are also examined and shown in Fig.5.1e and Fig.5.1f respectively. Both the spectra show the characteristics peaks for amine functional groups as well as for C−N stretching vibration mode. In the spectrum of rGO-PPD, the intensities of the bands related to the oxygen functionalities are found to decrease, implying the reduction of GO by PPD. In both spectra, peak appeared at 1171 cm^{-1} (Fig.5.1e) and 1167 cm^{-1} (Fig.5.1f) for C−N stretching vibration, which indicates successful functionalization of PPD into

both GO and CNT through C−NH−C linkage. Thus the results indicate obvious functionalization of PPD in the GO-CNT hybrid as the peak for C−N stretching vibration is present in both rGO-PPD and CNT-PPD components.

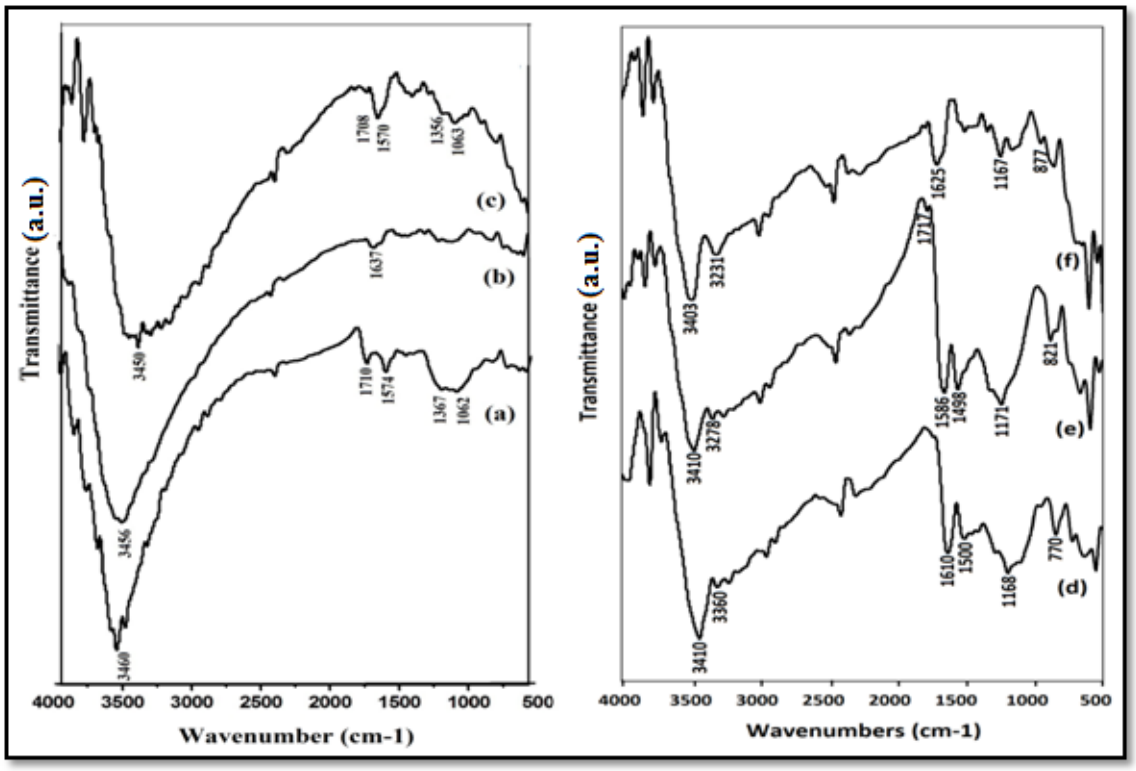

Fig.5.1 FTIR spectrum of (a) GO, (b) MWCNT, (c) GO–CNT (d) rGO-CNT-PPD (e) rGO-PPD and (f) CNT-PPD

5.3.1.2 XRD analysis

Fig.5.2 shows XRD patterns of GO, CNT, GO–CNT and rGO-CNT-PPD hybrid. Pristine graphite exhibits a strong crystalline peak at 26.5° for (002) plane [35]. However, GO exhibited the strong diffraction peak at $2\theta = 11.45^{o}$, which can be indexed as (001) reflection due to oxygen containing functional groups on carbon sheets. The XRD pattern of CNT displayed a sharp (002) peak at $2\theta = 25.15^{o}$. The XRD of GO–CNT hybrid exhibits a strong diffraction peak at $2\theta = 25.05^{o}$ for CNT. rGO-CNT-PPD exhibits a strong peak at $2\theta = 26.1°$ with slightly broadening nature. The strong peak at 26.1° is due to the presence of CNT and the broadening is due to their interactions confirming formation of rGO-CNT-PPD hybrid.

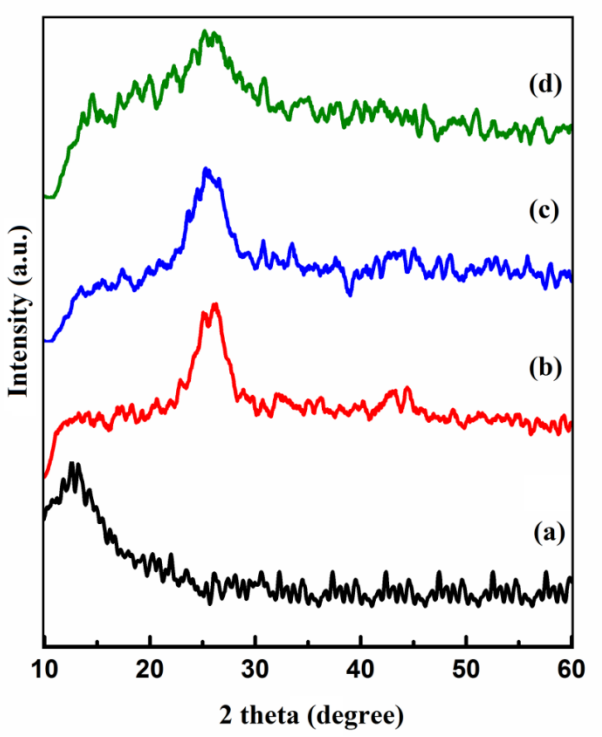

Fig.5.2 XRD patterns of (a) GO, (b) CNT, (c) GO-CNT and (d) rGO-CNT-PPD

5.3.1.3 SEM analysis

A salient difference in surface morphology between GO-CNT and rGO-CNT-PPD hybrid is observed (Fig.5.3). The SEM image of GO-CNT revealed that the GO sheets were entirely wrapped by the tubular networks of CNT confirming that the incorporation of CNT into GO (Fig.5.3a). While after functionalization with PPD, a rough morphology of the surface of the hybrid was observed indicating functionalization of the hybrid (Fig.5.3b).

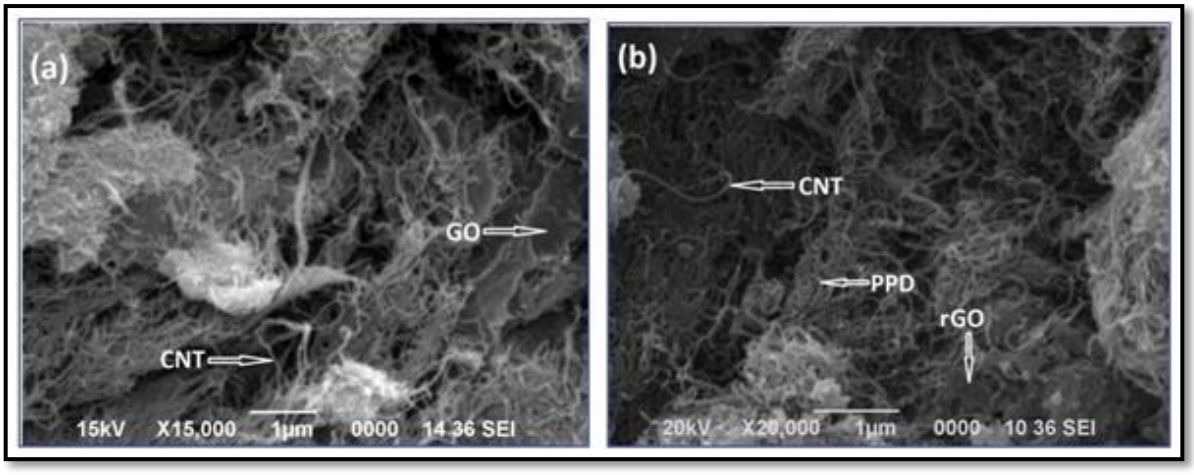

Fig.5.3 SEM images of (a) GO-CNT and (b) rGO-CNT-PPD hybrid

5.3.1.4 TEM analysis

TEM images GO-CNT and rGO-CNT-PPD hybrid are shown in Fig.5.4. TEM image of GO-CNT hybrid (Fig.5.4a) revealed that nanotubes were attached on the GO sheet without large bundles or aggregates. However, a different morphology is observed in (Fig.5.4b). Some dark spots appeared on the surface of GO-CNT hybrid due to the presence of PPD. Thus the image confirms successful functionalization of the hybrid by PPD.

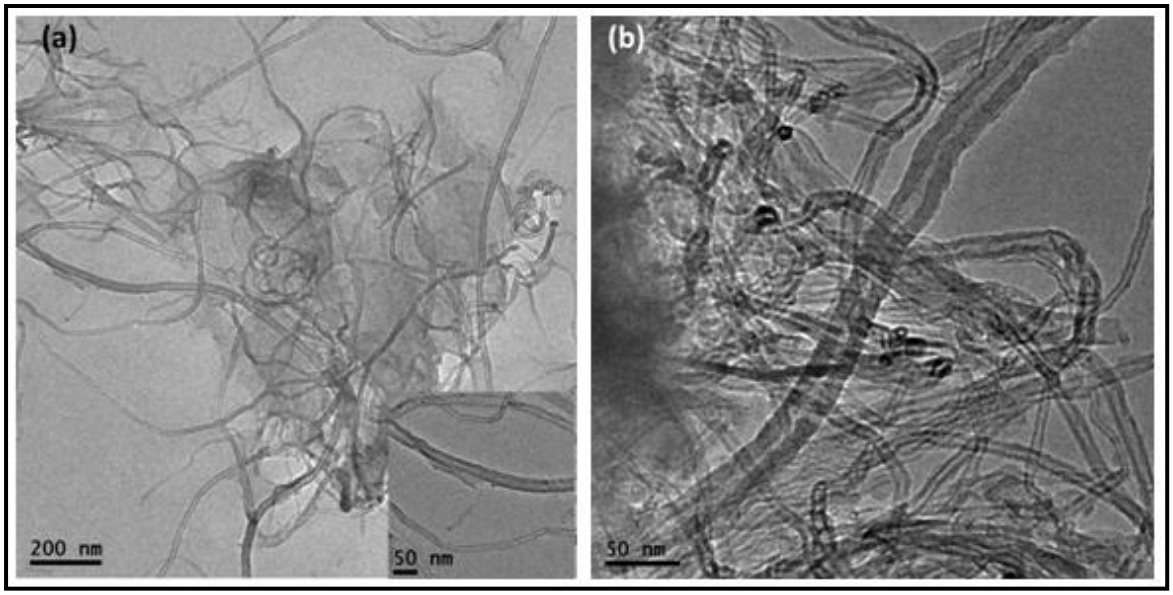

Fig.5.4 TEM images of (a) GO-CNT and (b) rGO-CNT-PPD hybrid. Inset in (a) is the TEM image of GO-CNT hybrid at higher resolution (50 nm).

5.3.2 Adsorption equilibrium and Kinetics study

Equilibrium studies of MV and MO were performed at room temperature at pH 7.0 and 3.0 respectively. Kinetic study was investigated to understand the mechanism of adsorption. To find out the minimum time required for adsorption to reach the steady state, effect of contact time was carried out. Contact time is the time after which the value of q_e remains same, i.e. after this time no increase or decrease in q_e value is observed. It can be seen in Fig.5.5 that the adsorption capacity of rGO-CNT-PPD hybrid increased instantly within first 20 min and thereafter proceed slowly until the steady state is reached within 120 min which indicates very fast adsorption kinetics of the dyes on the hybrid. After 120 min the value of q_e did not change. On the basis of the above result, a

contact time of 120 min was selected for both cases for a sure establishment of the adsorption equilibrium in further adsorption studies. At pH 7.0, the value of q_e for adsorption of MV was found to be 299 mg/g at steady state, whereas at pH 3.0, the value was 294 mg/g due to adsorption of MO.

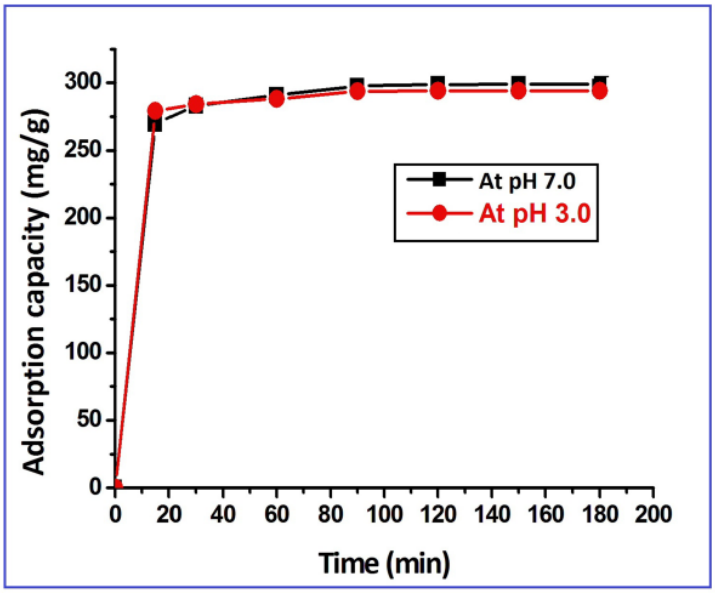

Fig.5.5 Effect of contact time on adsorption capacity at pH 7.0 and pH 3.0 onto rGO-CNT-PPD hybrid

In order to investigate the detailed characteristics of the adsorption phenomenon, two conventional kinetic models, pseudo-first-order and pseudo-second-order kinetic model were applied to identify the dynamic of the adsorption process. The pseudo-first-order model can be expressed as [38]

$$\log(q_e - q_t) = \log q_e - k_1 t/2.303 \quad (3)$$

where q_e and q_t are the adsorbed dye amounts on hybrid at equilibrium and at various times t (mg/g), respectively. k_1 is the rate constant of the pseudo-first-order model of adsorption (min^{-1}).

The pseudo-second-order model can be expressed as [39]

$$t/q_t = 1/k_2 q_e^2 + t/q_e \quad (4)$$

where q_e and q_t are defined as in the pseudo-first-order model and k_2 is the rate constant of the pseudo-second-order model of adsorption (g/mg.min). The values of q_e and k_2 can be calculated from the slope and intercept of the linear plot of t/q_t against t.

Kinetic parameters and correlation coefficients (R^2) are summarized in Table 5.1. The R^2 values for the pseudo-second-order model at pH 7.0 and pH 3.0 are 1, whereas for the pseudo-first-order model values are 0.946 and 0.923 respectively. Again, the experimental adsorption capacity ($q_{e,exp}$) values at both pH of the pseudo-first-order model were also very close to the calculated adsorption capacity ($q_{e,cal}$). Thus these results suggest that pseudo-second-order kinetic model fit the adsorption of MV as well as MO on rGO-CNT-PPD hybrid at pH 7.0 and 3.0 respectively.

Table 5.1 Kinetic Parameters for the adsorption of MV onto rGO-CNT-PPD hybrid at different pH.

Dye	pH	pseudo-first-order kinetics				pseudo-second-order kinetics		
		$q_{e,exp}$ (mg/g)	k_1 (min^{-1})	$q_{e,cal}$ (mg/g)	R^2	k_2 ($gmg^{-1}\,min^{-1}$)	$q_{e,cal}$ (mg/g)	R^2
MV	7.0	298	0.046	74.7	0.945	1.86×10^{-3}	333.33	1
MO	3.0	294	0.048	46.77	0.923	2.89×10^{-3}	333.33	1

5.3.3 Adsorption isotherms

The adsorption isotherm models provide information on the interaction between the adsorbent and the adsorbate when the adsorption process reaches equilibrium. Langmuir and Freundlich isotherms models were used to analyze adsorption equilibrium. The Langmuir isotherm theory assumes that adsorption cannot proceed beyond monolayer coverage of adsorbate over a homogeneous adsorbent surface and there are no interactions between adsorbed molecules. The Freundlich isotherm is an empirical equation based on multilayer adsoption on heterogeneous surface. The equations of linearized Langmuir isotherm (eqn. 5) and Freundlich (eqn. 6) adsorption isotherm models are given below [40, 41]

$$C_e/q_e = C_e/q_m + 1/q_m K_L \quad (5)$$

$$\ln q_e = (1/n)\ln C_e + \ln K_F \quad (6)$$

Where, C_e is the equilibrium concentration of the dye in solution (mg/L), q_e is the adsorbed dye amount per gram of the hybrid (mg/g), q_m represents the maximum

adsorption capacity of the adsorbent (mg/g), K_L and K_F are the Langmuir and Freundlich constants which are related to the affinity of the binding sites and adsorption capacity, respectively. The values of q_m and K_L can be calculated from the slope and intercept of the linear plot of C_e/q_e versus C_e. n represents the adsorption intensity; if n > 1, indicating a favorable condition for adsorption. The values of K_F and n can be obtained from the intercept and slope of the linear plot of ln q_e against ln C_e.

The parameters and correlation coefficients of both isotherm models at pH 7.0 and pH are summarized in Table 5.2. At both pH, it can be seen that the adsorption capacity increases with increase in initial dye concentration. As concentration increases, driving force from concentration gradient increases which accelerates the diffusion speed of dyes toward rGO-CNT-PPD hybrid. The better fitting by the Langmuir isotherm for both cases demonstrates that a monolayer adsorption process has taken place on the surface of the rGO–CNT-PPD hybrid and there is no subsequent interaction between adsorbed species.

Table 5.2 Isotherm Parameters for the adsorption of MV and MO by rGO–CNT-PPD hybrid at different pH

Dye	pH	Langmuir isotherm				Freundlich isotherm		
		T(K)	q_m(mg/g)	K_L(L/mg)	R^2	K_F	n	R^2
MV	7.0	298	333.33	0.67	0.992	150.66	3.86	0.713
MO	3.0	298	333.33	0.33	0.999	187.35	2.39	0.69

5.3.4 Effect of the pH

Solution pH is one of the most important factors in determining the adsorption properties of an adsorbent because it can change the net charge of the adsorbent and adsorbate. Fig.6a shows the effect of the solution pH on MO-MV mixture adsorption by rGO-CNT-PPD hybrid with the initial pH ranging from 1.0 to 11.0. At different pH, concentration of dyes after adsorption was measured by uv-visible spectroscopy at two different wavelengths, 464 nm and 582 nm. At 464 nm, the value of q_e is highest (294 mg/g) at pH 3.0, while q_e decreases sharply from pH 7.0 onwards. While at 582 nm, the hybrid showed a little change in adsorption capacity (around 294 mg/g) in pH range from

6.0 to 11.0 and maximum at pH 7.0 (298.5mg/g), while at pH 3.0, the adsorption capacity declined sharply and even reached to 27.5 mg/g (at 582 nm wavelength). Again, the uv-vis spectrum (Fig.6b) shows that at pH 7.0, there is no peak at 582 nm wavelength for MV, while at pH 3.0, peak for MO at 464 nm disappeared completely. These results indicated that at pH 7.0, the adsorbent can remove MV and at pH 3.0, the adsorbent selectively removes MO from the mixture of MO-MV solution. For these reasons all other experiment were carried out at pH 7.0 and 3.0 to remove MV and MO respectively.

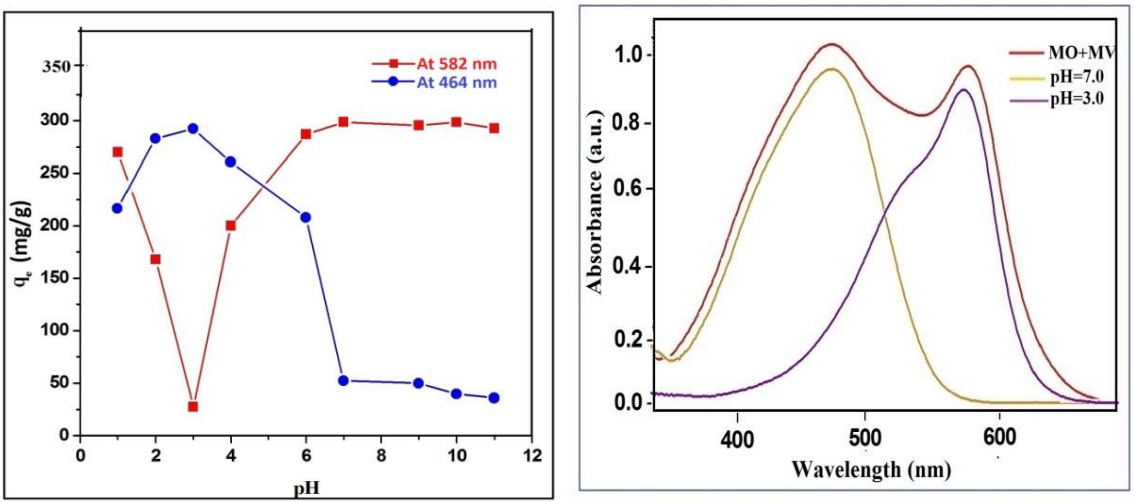

Fig.5.6 (a) Effect of pH on adsorption of MV-MO mixture on rGO-CNT-PPD hybrid at 464 nm and 582 nm and (b) uv-visible spectra of MO+MV solution before adsorption (red), after adsorption at pH 7.0(yellow) and at pH 3.0(violet).

The effect of pH on selective adsorption of MO and MV from their mixture is shown scheme 5.1. At pH 7.0, rGO-CNT-PPD hybrid can remove 99.5% MV selectively from the mixture which is due to the electrostatic interaction between the adsorbent and the cationic dye MV. Nitrogen atoms of PPD can offer their lone pairs of electrons as well as the unreduced oxygen containing functional groups of GO effectively attract the cationic dye. While at pH 3.0, the hybrid can remove MO selectively with 98% removal efficiency. At this pH, concentration of hydrogen ion increases which neutralizes the negative charges of the hybrid facilitating adsorption of anionic MO.

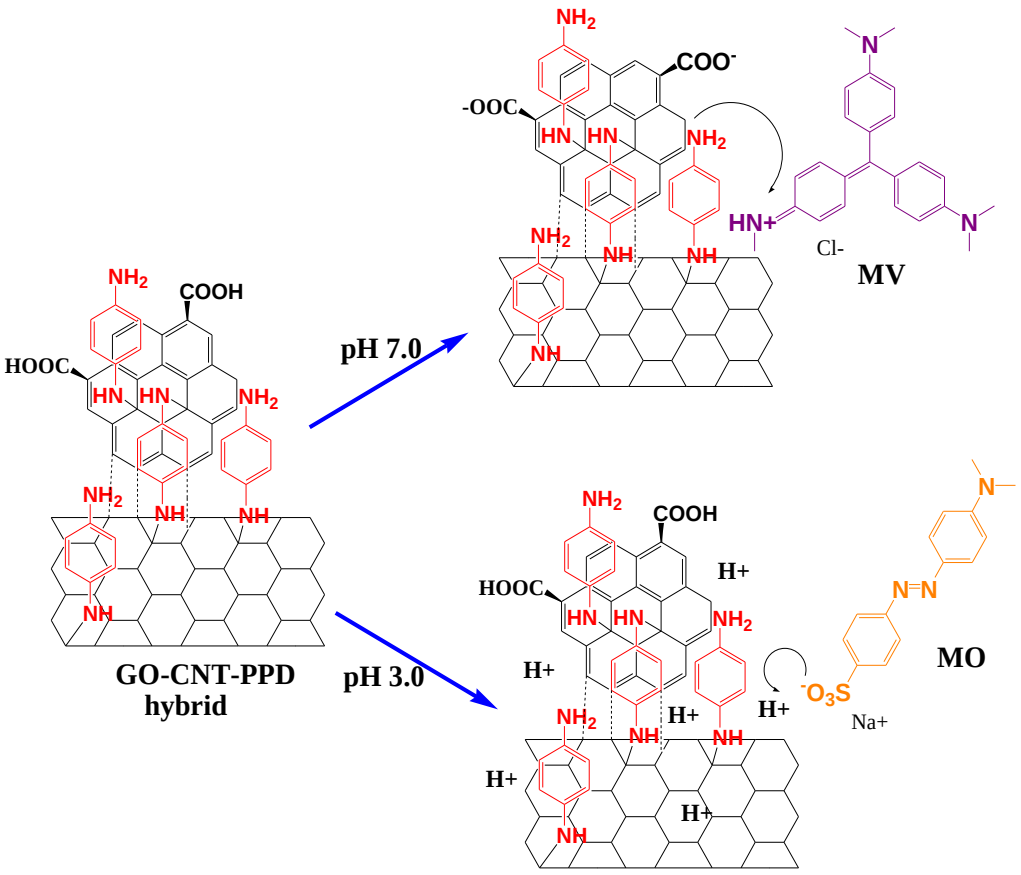

Scheme 5.1 Effect of pH on adsorption of MV and MO.

5.3.4 Regeneration of the rGO-CNT-PPD hybrid

The adsorbent can be easily regenerated and reused for further adsorption-desorption cycles. To evaluate the reusability of the rGO–CNT-PPD hybrid, further adsorption–desorption experiments were carried out at pH 7. Fig.6 shows that the removal percentage of MV from the mixture remains almost same even after five cycles.

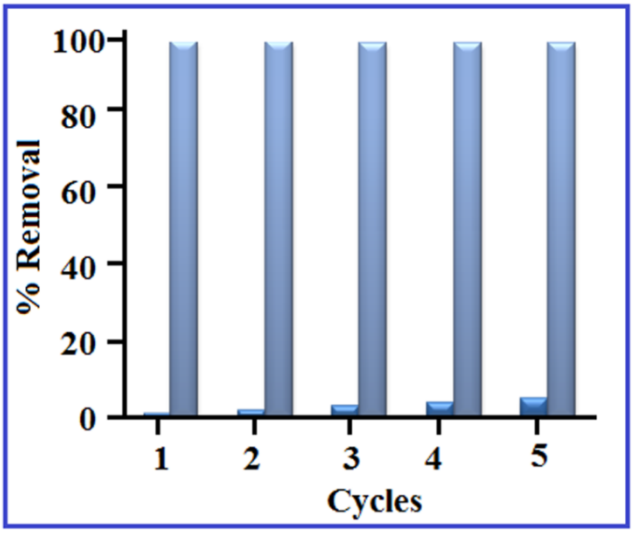

Fig. 5.7 Removal efficiency of MV at pH 7.0 on rGO-CNT-PPD hybrid in different cycles

5.4 Selective dye adsorption

As far our knowledge, there is no reported work for selective adsorption of MV and MO from their mixture. Ho, K. Y. et al. [26] used two different adsorbents (OMS-NH_2 and OMS-COOH) for selective adsorption of two differently charged dyes from their mixture. On the other hand, in our study, using same adsorbent selective adsorption of a cationic and an anionic dye was carried out by simply changing the pH of the solution. The adsorbent selectively adsorbed one dye at certain pH without changing the concentration of another dye. The adsorption capacity of rGO-CNT-PPD hybrid displayed significantly higher values for the mixture compared to earlier reported values of single dye adsorption [42, 43]. Table 5.3 shows the comparisons of maximum adsorption capacities of the rGO–CNT-PPD hybrid obtained in this study with various adsorbents previously used for the adsorption of MV and MO.

Table 5.3 Comparison of adsorption capacities of MV and MO onto various adsorbents

Dye	Adsorbents	Adsorption capacity (mg/g)	References
MV	GO-CNT-PPD hybrid	298	This work
	CNT chemically bonded to rGO	245	42
	Magnetic modified MWCNT	228	44
	Phosphoric acid activated carbon	60.42	45
	Sulphuric acid activated carbon	85.84	45
	Granular activated carbon	95	46
MO	GO-CNT-PPD hybrid	294	This work
	Mesoporous carbon materials	294.1	47
	Activated carbon modified by silver nano particlec	27.48	43

5.5 Conclusion

GO-CNT hybrid was successfully functionalized with simultaneous reduction of the hybrid with PPD. Its adsorption capacity was investigated systematically towards removal of MV and MO selectively from their aqueous mixture. The adsorption capacity was highly dependent on the pH and temperature of the solution. At pH 7.0, due to the electrostatic interaction between the nitrogen atoms of amine functional groups the unreduced oxygen containing functional groups of adsorbent and the cationic dye, rGO-CNT-PPD hybrid can remove 99.5% MV selectively from the mixture of MV-MO solution. While at pH 3.0, it can remove MO selectively having 98% removal efficiency due to the increase in hydrogen ion concentration facilitating adsorption of anionic MO. In view of the easy method of the preparation of the adsorbent, its reusability and its excellent selectivity towards dye adsorption, this hybrid is an important tool in remediation technology.

5.6 References

[1] Azim, W., Sani, R. K., and Banerjee, U. C. Biodegradation of triphenylmethane dyes. *Enzyme and microbial technology,* 22(3)185-191, 1998.

[2] Arami, M., Limaee, N. Y., Mahmoodi, N. M., and Tabrizi, N. S. Equilibrium and Kinetic studies for the adsorption of direct and acid dyes from aqueous solution by soy meal hull. *Journal of Hazardous Materials,* 135(1-3):171–179, 2006.

[3] Vandevivere, P., Bianchi, C., and Verstaete, R. W. Treatment and reuse of wastewater from the textile wet processing industry: Review of emerging technologies. *Journal of Chemical Technology & Biotechnology: International Research in Process, Environmental AND Clean Technology,* 72:289-302, 1998.

[4] Zhang, Y., Causserand, C., Aimar, P., and Cravedi, J. P. Removal of bisphenol A by a nanofiltration membrane in view of drinking water production. *Water research,* 40(20):3793-3799, 2006.

[5] Wang, R., Ren, D., Xia, S., Zhang, Y., and Zhao, J. Photocatalytic degradation of Bisphenol A (BPA) using immobilized TiO_2 and UV illumination in a horizontal circulating bed photocatalytic reactor (HCBPR). *Journal of Hazardous Materials,* 169(1-3):926-932, 2009.

[6] Selcuk, H. Decolorization and detoxification of textile wastewater by ozonation and coagulation processes. *Dyes and Pigments,* 64(3):217-222, 2005.

[7] Dutta, K., Mukhopadhyay, S., Bhattacharjee, S., and Chaudhuri, B. Chemical oxidation of methylene blue using a Fenton-like reaction. *Journal of hazardous materials,* 84(1):57-71, 2001.

[8] Hassan, M. M. and Hawkyard, C. J. Reuse of spent dyebath following decolorisation with ozone. *Coloration technology,* 118(3):104-111, 2002.

[9] Liu, C. H., Wu, J. S., Chiu, H. C., Suen, S. Y., and Chu, K. H. Removal of anionic reactive dyes from water using anion exchange membranes as adsorbers. *Water Research,* 41(7):1491-1500, 2007.

[10] Jørgensen, S. E. Examination of the applicability of cellulose ion exchangers for water and waste water treatment. *Water Research,* 13(12):1239-1247, 1979.

[11] Blackburn, R. S. Natural polysaccharides and their interactions with dye molecules: applications in effluent treatment. *Environmental science & technology,* 38(18):4905-4909, 2004.

[12] Liu, G., Ma, J., Li, X., and Qin, Q. Adsorption of bisphenol A from aqueous solution onto activated carbons with different modification treatments. *Journal of hazardous materials,* 164(2-3):1275-1280, 2009.

[13] Kuo, C. Y. Comparison with as-grown and microwave modified carbon nanotubes to removal aqueous bisphenol A. *Desalination,* 249(3):976-982, 2009.

[14] Asada, T., Oikawa, K., Kawata, K., Ishihara, S., Iyobe, T., and Yamada, A. Study of removal effect of bisphenol A and β-estradiol by porous carbon. *Journal of health science,* 50(6):588-593, 2004.

[15] Ramesha, G. K., Kumara, A. V., Muralidhara, H. B., and Sampath, S. Graphene and graphene oxide as effective adsorbents toward anionic and cationic dyes. *Journal of colloid and interface science,* 361(1):270-277, 2011.

[16] Schlierf, A., Yang, H., Gebremedhn, E., Treossi, E., Ortolani, L., Chen, L., Minoia, A., Morandi, V., Samorì, P., Casiraghi, C., and Beljonne, D., Nanoscale insight into the exfoliation mechanism of graphene with organic dyes: effect of charge, dipole and molecular structure. *Nanoscale,* 5(10):4205-4216, 2013.

[17] Xu, J., Wang, L., and Zhu, Y. Decontamination of bisphenol A from aqueous solution by graphene adsorption. *Langmuir,* 28(22):8418-8425, 2012.

[18] Zhao, J., Ren, W., and Cheng, H. M. Graphene sponge for efficient and repeatable adsorption and desorption of water contaminations. *Journal of Materials Chemistry,* 22(38):20197-20202, 2012.

[19] Fletcher, A. J., Yüzak, Y., and Thomas, K. M. Adsorption and desorption kinetics for hydrophilic and hydrophobic vapors on activated carbon. *Carbon,* 44(5):989-1004, 2006.

[20] Ghaedi, M., Hassanzadeh, A., and Kokhdan, S. N., Multiwalled carbon nanotubes as adsorbents for the kinetic and equilibrium study of the removal of alizarin red S and morin. *Journal of Chemical & Engineering Data,* 56(5):2511-2520, 2011.

[21] Machado, F. M., Bergmann, C. P., Lima, E. C., Royer, B., de Souza, F. E., Jauris, I. M., Calvete, T., and Fagan, S. B. Adsorption of Reactive Blue 4 dye from water solutions by carbon nanotubes: experiment and theory. *Physical Chemistry Chemical Physics,* 14(31):11139-11153, 2012.

[22] Wang, S., Ng, C. W., Wang, W., Li, Q., and Li, L. A comparative study on the adsorption of acid and reactive dyes on multiwall carbon nanotubes in single and

binary dye systems. *Journal of Chemical & Engineering Data,* 57(5):1563-1569, 2012.

[23] Bradder, P., Ling, S. K., Wang, S., and Liu, S. Dye adsorption on layered graphite oxide. *Journal of Chemical & Engineering Data,* 56(1):138-141, 2010.

[24] Li, D., Müller, M. B., Gilje, S., Kaner, R. B., and Wallace, G. G. Processable aqueous dispersions of graphene nanosheets. *Nature nanotechnology*, 3(2):101−105, 2008.

[25] Sharma, P. and Das, M. R. Removal of a cationic dye from aqueous solution using graphene oxide nanosheets: investigation of adsorption parameters. *Journal of Chemical & Engineering Data,* 58(1):151-158, 2012.

[26] Ho, K. Y., McKay, G. and Yeung, K. L., Selective adsorbents from ordered mesoporous silica. *Langmuir,* 19(7):3019-3024, 2003.

[27] Cai, D., Song, M., and Xu, C. Highly Conductive Carbon-Nanotube/Graphite-Oxide Hybrid Films, *Advanced Materials,* 20(9), 1706-1709, 2008.

[28] Aboutalebi, S. H., Chidembo, A. T., Salari, M., Konstantinov, K., Wexler, D., Liu, H. K., and Dou, S. X. Comparison of GO, GO/MWCNTs composite and MWCNTs as potential electrode materials for supercapacitors. *Energy & Environmental Science,* 4(5):1855-1865, 2011.

[29] Kim, Y. K., Na, H. K., Kwack, S. J., Ryoo, S. R., Lee, Y., Hong, S., Hong, S., Jeong, Y., and Min, D. H. Synergistic effect of graphene oxide/MWCNT films in laser desorption/ionization mass spectrometry of small molecules and tissue imaging. *Acs Nano,* 5(6):4550-4561. 2011.

[30] Wang, R., Sun, J., Gao, L., Xu, C., Zhang, J., and Liu, Y. Effective post treatment for preparing highly conductive carbon nanotube/reduced graphite oxide hybrid films. *Nanoscale,* 3(3):904-906, 2011.

[31] Huang, Z. D., Zhang, B., Oh, S. W., Zheng, Q. B., Lin, X. Y., Yousefi, N., and Kim, J. K. Self-assembled reduced graphene oxide/carbon nanotube thin films as electrodes for supercapacitors. *Journal of Materials Chemistry,* 22(8):3591-3599, 2012.

[32] Kemp, K. C., Seema, H., Saleh, M., Le, N. H., Mahesh, K., Chandra, V., and Kim, K. S. Environmental applications using graphene composites: water remediation and gas adsorption. *Nanoscale,* 5(8):3149-3171, 2013.

[33] Stankovich, S., Dikin, D. A., Piner, R. D., Kohlhaas, K.A., Kleinhammes, A., Jia, Y., Wu, Y., Nguyen, S. T., and Ruoff, R. S. Synthesis of graphene-based nanosheets via chemical reduction of exfoliated graphite oxide. *Carbon,* 45(7):1558-1565, 2007.

[34] Shin, H. J., Kim, K. K., Benayad, A., Yoon, S. M., Park, H. K., Jung, I. S., Jin, M. H., Jeong, H. K., Kim, J. M., Choi, J. Y., and Lee, Y. H. Efficient reduction of graphite oxide by sodium borohydride and its effect on electrical conductance. *Advanced Functional Materials,* 19(12):1987-1992, 2009.

[35] Kim, N. H., Kuila, T., and Lee, J. H. Simultaneous reduction, functionalization and stitching of graphene oxide with ethylenediamine for composites application. *Journal of Materials Chemistry A,* 1(4):1349-1358, 2013.

[36] Wang, B., Luo, B., Liang, M., Wang, A., Wang, J., Fang, Y., Chang, Y., and Zhi, L. Chemical amination of graphene oxides and their extraordinary properties in the detection of lead ions. *Nanoscale,* 3(12):5059-5066, 2011.

[37] William, S., Hummers, Jr., and Offeman, R. E. Preparation of graphitic oxide. *Journal of the American Chemical Society,* 80(6):1339-1339, 1958.

[38] Ho, Y. S. and McKay, G. Sorption of dye from aqueous solution by peat. *Chemical engineering journal,* 70(2):115-124, 1998.

[39] Weber, W. J. and Morris, J. C. Kinetics of adsorption on carbon from solution. *Journal of the Sanitary Engineering Division,* 89(2):31-60, 1963.

[40] Langmuir, I. The constitution and fundamental properties of solids and liquids. Part I. Solids. *Journal of the American chemical society,* 38(11):2221-2295, 1916.

[41] Freundlich, H. Concerning adsorption in solutions. *Journal of Physical Chemistry,* 57:385−471, 1906.

[42] Kotal, M. and Bhowmick, A. K. Multifunctional hybrid materials based on carbon nanotube chemically bonded to reduced graphene oxide. *The Journal of Physical Chemistry C,* 117(48):25865-25875, 2013.

[43] Pal, J., Deb, M. K., Deshmukh, D. K., and Verma, D. Removal of methyl orange by activated carbon modified by silver nanoparticles. *Applied Water Science,* 3(2):367-374, 2013.

[44] Madrakian, T., Afkhami, A., Ahmadi, M., and Bagheri, H. Removal of some cationic dyes from aqueous solutions using magnetic-modified multi-walled carbon nanotubes. *Journal of hazardous materials,* 196:109-114, 2011.

[45] Senthilkumaar, S., Kalaamani, P., and Subburaam, C. V. Liquid phase adsorption of crystal violet onto activated carbons derived from male flowers of coconut tree. Journal of hazardous materials, 136(3):800-808, 2006.

[46] Azizian, S., Haerifar, M., and Bashiri, H. Adsorption of methyl violet onto granular activated carbon: Equilibrium, kinetics and modeling. *Chemical Engineering Journal,* 146(1):36-41, 2009.

[47] Mohammadi, N., Khani, H., Gupta, V. K., Amereh, E., and Agarwal, S., Adsorption process of methyl orange dye onto mesoporous carbon material–kinetic and thermodynamic studies. *Journal of colloid and interface science,* 362(2):457-462, 2011.